

Decay rates of magnetic modes below the threshold of a turbulent dynamo

J. Herault, F. Pétrélis, and S. Fauve

Laboratoire de Physique Statistique, Ecole Normale Supérieure, CNRS, Université P. et M. Curie, Université Paris Diderot, Paris, France

(Received 9 December 2013; published 4 April 2014)

We measure the decay rates of magnetic field modes in a turbulent flow of liquid sodium below the dynamo threshold. We observe that turbulent fluctuations induce energy transfers between modes with different symmetries (dipolar and quadrupolar). Using symmetry properties, we show how to measure the decay rate of each mode without being restricted to the one with the smallest damping rate. We observe that the respective values of the decay rates of these modes depend on the shape of the propellers driving the flow. Dynamical regimes, including field reversals, are observed only when the modes are both nearly marginal. This is in line with a recently proposed model.

DOI: [10.1103/PhysRevE.89.043004](https://doi.org/10.1103/PhysRevE.89.043004)

PACS number(s): 47.65.–d

The generation of magnetic field by the flow of an electrically conducting fluid through the dynamo process has been primarily studied in order to understand planetary and stellar magnetic fields [1]. This phenomenon also provides a canonical example of an instability that occurs on a fully turbulent flow. Instabilities occurring on turbulent flows involve several fundamental open questions, such as the characterization of growing or decaying eigenmodes in the linear regime or the possibly anomalous scaling of the moments of the magnetic field amplitude versus the distance to instability threshold in the nonlinear regime [2,3]. We present here an experimental study related to the former aspect.

The threshold of a linear instability of a stationary or time-periodic state is reached when the largest growth rate (eigenvalue) of the eigenmodes of the evolution equation for the perturbations vanishes. Below this threshold, small perturbations decay exponentially with a decay rate proportional to the corresponding eigenvalue. The value of the decay rate thus measures the distance to the threshold of linear instability of the corresponding eigenmode. Measurements of growth and decay rates are commonly performed to characterize instabilities. Eigenmodes with different symmetries are not linearly coupled, and depending on the symmetries of the initial conditions, their decay rate can be measured. The problem is more complex for an instability generated by a turbulent flow. First, although growth and decay can be characterized by a Lyapunov exponent, eigenmodes cannot be defined in the usual way. In the limit of small turbulent fluctuations about the mean flow, one can consider the eigenmodes of the mean flow as a first approximation, as done in the past for the dynamo problem [4]. However, it has been shown both experimentally [5] and from numerical simulations [6] that the magnetic field generated by a turbulent flow can strongly differ from a prediction based on the mean flow alone. In addition, even if some modes are defined in an appropriate way, turbulent fluctuations can transfer energy from one mode to the other, thus contaminating decay rate measurements. We report an experimental procedure to define these modes and avoid this bias by independently measuring the decay rate of the two less damped modes with different symmetries. We then show how their difference in decay rates can be related to the dynamics observed above instability threshold.

The experiment concerns the generation of a magnetic field by a von Karman flow of liquid sodium (VKS experiment) that has been already reported in detail elsewhere [7]. The flow is

driven by two counter-rotating coaxial propellers in a cylinder containing roughly 160 liters of liquid sodium maintained at a temperature around 120° C for which the electrical conductivity σ is close to 10^7 (Ωm)⁻¹ (See Fig. 1). The propellers are soft iron disks fitted with curved (resp. straight) iron blades. When they counter rotate with the same speed, the dynamo threshold is reached for $F_1 = F_2 = 13$ Hz (resp. 19 Hz). This corresponds to a magnetic Reynolds number, $R_m = 2\pi\mu_0\sigma R^2 F$ around 24 (resp. 35) where $R = 154.5$ mm is the radius of the disks. The time-averaged magnetic field is roughly an axial dipole whose amplitude displays a slightly imperfect bifurcation because of the remanent magnetization of the disks. When the disks counter rotate at different frequencies, a mode of quadrupolar symmetry is also generated [5]. The dipole and the quadrupole have opposite symmetries with respect to a rotation of π around the z axis in the midplane between the disks (\mathcal{R}_π as sketched in Fig. 1). For a large enough frequency difference, dynamical regimes can be observed such as periodic or random reversals of the magnetic field [5,8] that involve energy transfers between the dipole and the quadrupole [9].

From now on, we restrict to measurements performed for exact counter rotation $F_1 = F_2 = F$. Below the onset of instability, we apply a magnetic field generated by two axial coils. Each coil carries an equal electric current flowing in the same (resp. opposite) direction, thus providing a Helmholtz (resp. anti-Helmholtz) configuration generating an axial field of dipolar (resp. quadrupolar) symmetry, i.e., odd (resp. even) under \mathcal{R}_π . The magnetic field is measured with two probes located close to the disks, 109 mm away from the midplane. Each probe measures the three components of the magnetic field at ten positions (the deepest probe is 103 mm away from the cylinder axis and the distance between probes is 28 mm).

We apply a time-periodic magnetic field with a square wave shape in order to measure the decay rate of the magnetic response below the dynamo threshold as performed in Refs. [10] and [11]. Experiments typically involve 20 periods of duration 10 s. When the external magnetic field is on, we observe a field induced by the flow of liquid sodium. When the external field is switched off, the induced magnetic field decays and reaches a small value that results from the ambient field. A first way to evaluate the amplitude of the excited magnetic mode is to calculate its energy density defined as the sum over the probes of the local energy density B_i^2 averaged over the different realizations. This method is accurate when

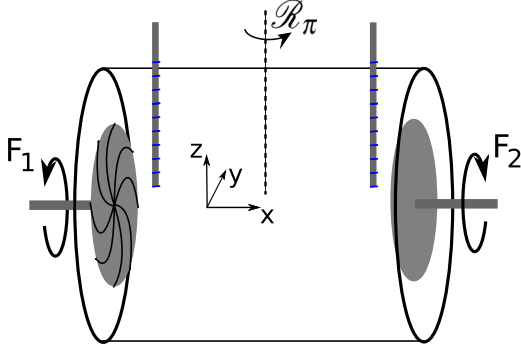


FIG. 1. (Color online) Sketch of the experiment: two impellers counter rotate at frequencies F_1 and F_2 . When $F_1 = F_2$ the setup is invariant to \mathcal{R}_π rotation. The vertical thick lines indicate the locations of the two arrays of three-axis Hall probes which measure the magnetic field close to each disk.

the field is dominated by a single mode. In Fig. 2, the time series is displayed for an anti-Helmholtz configuration such that one may expect to measure the decay rate of the quadrupolar mode. The decay of the magnetic energy is not exponential (black curve) and as will be made clear below, the time recording actually transitions between two different exponential behaviors. In this case, the decay rate is not correctly measured from the evolution of the magnetic energy. The method that we present now solves this problem.

We note $\mathbf{B}_1(t)$ [resp. $\mathbf{B}_2(t)$] as the vectors defined using the 30 values measured by the 10 probes close to disk 1 (resp. 2). In order to extract the decay of the amplitude of unstable modes, we define two reference geometries noted \mathbf{B}_1^r and \mathbf{B}_2^r , which are the time averages of the vectors \mathbf{B}_1 and \mathbf{B}_2 when the dynamo is operating. The spatial structure given by \mathbf{B}_1^r and \mathbf{B}_2^r is a dipole, and it does not change significantly above the dynamo onset. Note that below the onset and for a field applied in the Helmholtz configuration the geometry of the induced magnetic field is quite similar to the dipole geometry \mathbf{B}_1^r and \mathbf{B}_2^r . Thus we could take indifferently either the spatial structure of the unstable mode or the one of the induced field to measure the decay rates. Therefore, this method can be applied even when the dynamo threshold has not been reached. The dipole and quadrupole amplitudes $D(t)$ and $Q(t)$ are defined by

$$\begin{aligned} D(t) &= \frac{1}{2} \left(\frac{\mathbf{B}_1 \cdot \mathbf{B}_1^r}{|\mathbf{B}_1^r|} + \frac{\mathbf{B}_2 \cdot \mathbf{B}_2^r}{|\mathbf{B}_2^r|} \right), \\ Q(t) &= \frac{1}{2} \left(\frac{\mathbf{B}_1 \cdot \mathbf{B}_1^r}{|\mathbf{B}_1^r|} - \frac{\mathbf{B}_2 \cdot \mathbf{B}_2^r}{|\mathbf{B}_2^r|} \right), \end{aligned} \quad (1)$$

where $|\mathbf{B}_i^r| = (\mathbf{B}_i^r \cdot \mathbf{B}_i^r)^{1/2}$. This amounts to a projection of the measured magnetic field on a reference spatial structure.

We show in Fig. 3 different realizations of the decay of $D(t)$ (in gray) for $F = 11$ Hz (the applied magnetic field is shut down at $t = 0$). The average over the different realizations $\bar{D}(t)$ (black curve) exhibits an exponential decay. \bar{D} is fitted with an exponential function $A \exp(-t/\tau) + \bar{D}_0$, where τ^{-1} is the decay rate and \bar{D}_0 is the amplitude of the dipole without applied magnetic field. Indeed, because of the imperfectness of the bifurcation, \bar{D}_0 is not exactly zero. It is created by

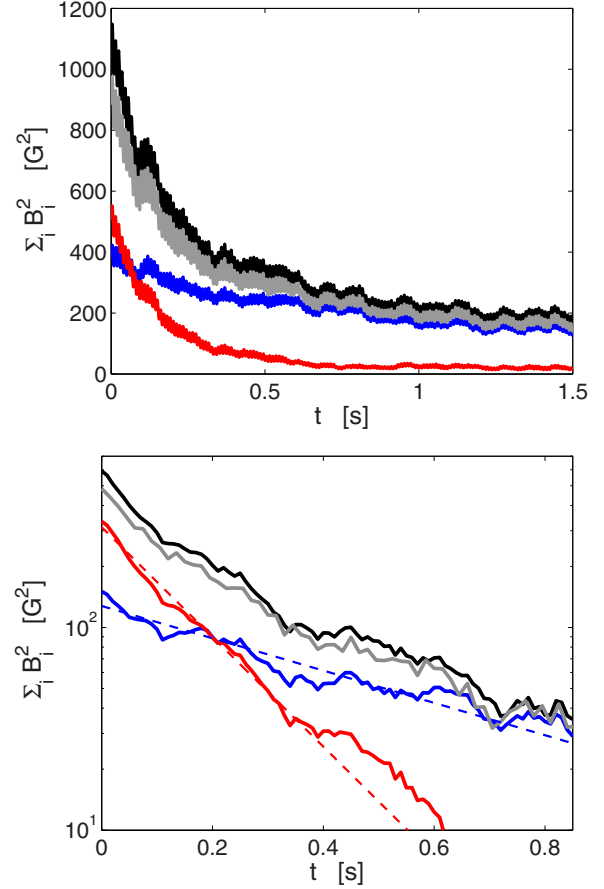


FIG. 2. (Color online) For an anti-Helmholtz applied magnetic field, time series of $(|B_1|^2 + |B_2|^2)/2$ (in black). Two behaviors are observed. The decay rate measured at initial time is the same as the one obtained from the quadrupolar projection (in red). At long time, it is the same as the one obtained from the dipolar projection (in blue). The gray curve represents the total amount of energy in the quadrupolar and dipolar modes. Top: lin-lin scale; bottom: log-lin scale, the long time value is subtracted so that exponential decays appear as straight lines.

the different sources of applied field (Earth's magnetic field, remanent magnetization of the disks, etc.).

The measured value of the decay rate is quite robust. As is displayed in the inset of Fig. 3, using the projection method, the same results are obtained for the decay rate of the dipole in the Helmholtz (resp. anti-Helmholtz) configuration. We now understand the behavior of the total energy displayed in Fig. 2 for an anti-Helmholtz applied field. At short time, the quadrupolar component is much larger than the dipolar one. The quadrupolar decay rate being larger than the dipolar one, after an initial phase (here of around 0.2 s), the energy of the quadrupolar component is drastically reduced and the dipolar component gives the main contribution to the energy. We note that the dipolar and the quadrupolar energy add up to nearly 80 percent of the total energy. All together, this explains why the time recording of the total energy crosses over between two different exponential behaviors. We also point out that a single configuration of applied field allows us to extract both decay rates because the projection disentangles the relative

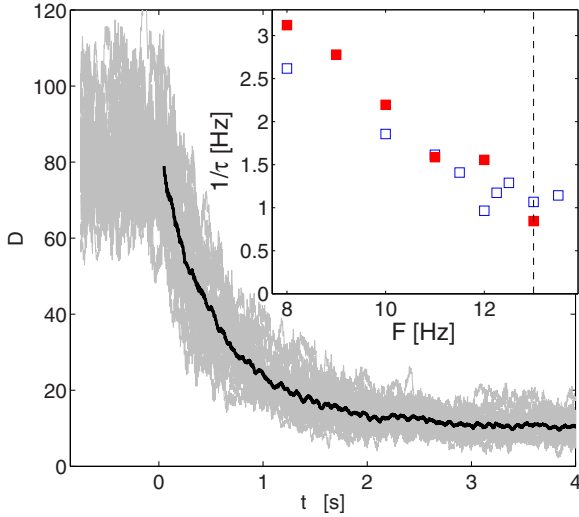


FIG. 3. (Color online) Decay of the amplitude of the dipolar projection for $F = 11$ Hz (applied field in the Helmholtz configuration). The thick black line is the average over the different realizations (displayed as thin gray lines). Inset: decay rate $1/\tau$ of the dipole as a function of the disk rotation frequency for an applied field in Helmholtz (\square) or anti-Helmholtz (\blacksquare) configuration.

contribution of each mode. This is mostly achievable with an applied field in the anti-Helmholtz configuration. Then a dominant part of the energy is initially injected in the most damped mode so that the slowest decaying mode is ultimately observed even though it has a small initial energy mostly due to imperfection in the experimental setup or in the symmetry of the applied field.

Trajectories in phase space also display the two successive behaviors, as shown in Fig. 4. When a field is applied in the anti-Helmholtz configuration, the trajectories wander around

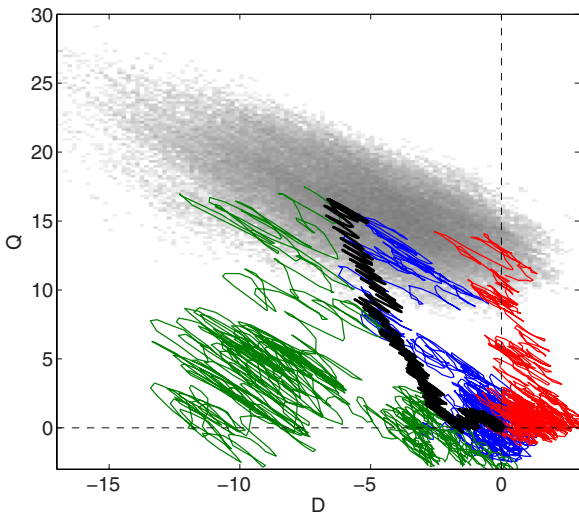


FIG. 4. (Color online) Phase space for the induced field (D, Q) for $F = 11$ Hz. The gray set contains the trajectories when a field is applied in the anti-Helmholtz configuration. The (colored online, thin) continuous curves are individual trajectories that start when the field is set to zero. The thick black curve is the average over the realizations.

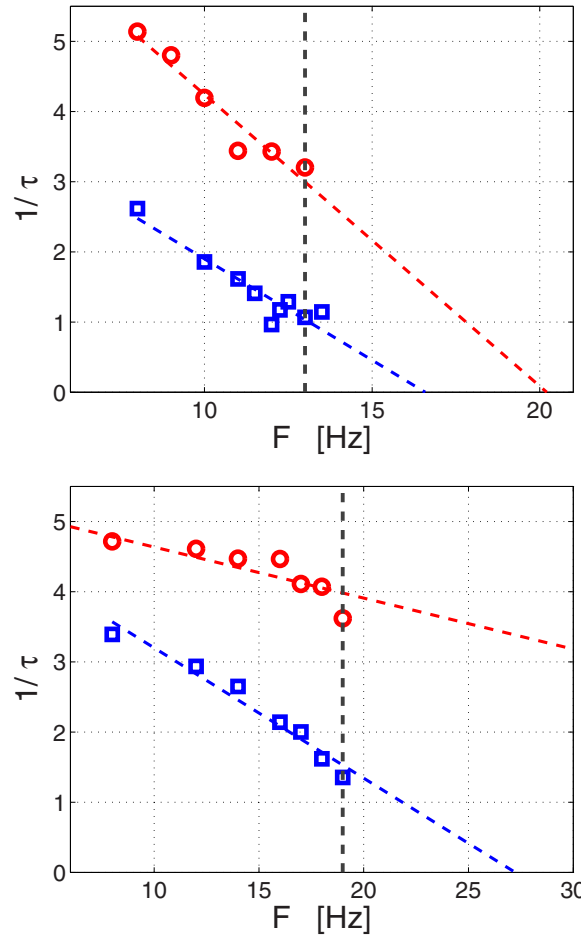


FIG. 5. (Color online) Decay rate of the dipolar mode (blue square) and of the quadrupolar mode (red circle) as a function of the rotation frequency. Upper panel: the flow is driven by disks with curved blades. Lower panel: the flow is driven by disks with straight blades.

a wide spot (in gray). Indeed turbulent fluctuations transfer energy between the modes. When the applied field is set to zero, the trajectories relax toward the origin. Turbulent fluctuations are also responsible for the observed large variability between the realizations. In contrast, the average over the realizations (thick black line) is simpler and is made of an evolution toward the $Q = 0$ axis followed by the evolution toward $D = Q = 0$. Despite the fluctuations, we thus can observe in phase space the two successive behaviors (decrease of the quadrupolar component followed by the decrease of the dipolar one).

We compare the decay rates for the dipolar and quadrupolar mode in Fig. 5. For disks fitted with curved blades (upper panel), we observe that at the onset ($F = 13$ Hz), the decay rate of the dipole has been reduced by a factor of 2.6 compared to its value at $F = 8$ Hz. The finite value of the decay rate measured at $F = 13$ Hz is probably biased by the imperfection of the bifurcation (see the discussion in Ref. [11]). We note that the decay rate of the quadrupolar mode has also been reduced from 5 s^{-1} to nearly 3 s^{-1} at the threshold. Within the accuracy of the measurements, the variations of the decay rates are linear in F in the range 8–13 Hz [12]. Both curves intersect the $1/\tau = 0$ line at comparable rotation frequencies close to 17 and 20 Hz, respectively.

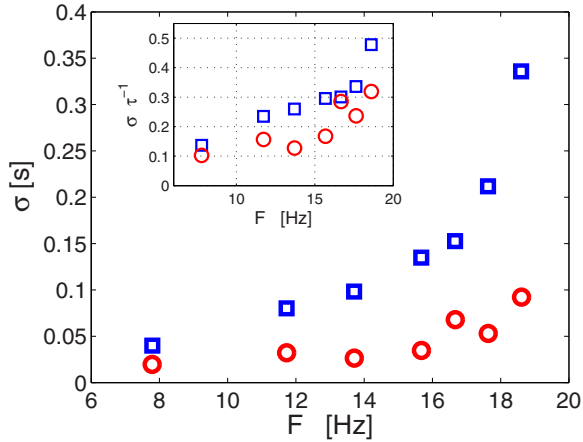


FIG. 6. (Color online) Standard deviation of the decay rate of the quadrupolar (red circle) and dipolar mode (blue square). In the inset, standard deviation over the mean.

A second set of experiments was performed with disks fitted with straight blades. In exact counter rotation, the onset takes place at a larger value $F = 19$ Hz. Between $F = 8$ Hz and the onset, the dipolar decay rate is reduced by a factor of 2.5. The amplitude of the variation is similar to the one observed in the case of disks fitted with curved blades. In contrast, the quadrupolar decay rate only varies from 4.8 s^{-1} to 3.6 s^{-1} . The linear fits of these curves cross the $1/\tau = 0$ line at $F = 27$ Hz for the dipolar mode and at F larger than 70 Hz for the quadrupolar one. We note that the estimated decay rates display strong fluctuations close to the dynamo threshold and thus can be sensitive to the fitting parameters. However, it is clear that the quadrupolar decay rate displays a stronger variation with F in the case of curved blades. Thus, at dynamo threshold, the quadrupolar mode is closer to its instability threshold when the flow is driven by curved blades.

These observations agree with the mechanism proposed to explain the dynamical regimes observed in the experi-

ments [13]. The dynamical regimes (e.g., random or periodic reversals) take place when both the dipolar and the quadrupolar modes are close to their onset of instability. Then breaking the forcing symmetry, i.e., rotating with F_1 different from F_2 , couples the two modes that can achieve a saddle-node bifurcation. Above this bifurcation, periodic reversals are observed while close to the threshold of the saddle-node bifurcation, turbulent fluctuations trigger random reversals. Reversals are observed when the effect of the symmetry breaking is comparable to the difference between the growth rates of the two modes. In the case of disks fitted with curved blades, the difference in values F at which $1/\tau$ reaches 0 is equal to $\Delta F \simeq 3$ Hz. Dynamical regimes of the magnetic field can be observed provided that $|F_1 - F_2|$ is larger than 3.25 Hz. In the case of disks fitted with straight blades, we have concluded from Fig. 5 that the difference between the growth rates is quite large. We thus expect that the breaking of symmetry will not be efficient enough to generate the saddle-node bifurcation. Indeed, this is confirmed by the experimental results since no dynamical regimes are actually observed with these disks. In other words, the flow driven by these disks generates modes with strongly different thresholds. Breaking the symmetry by rotating the disks at different speeds does not result in a strong enough coupling between the two modes so that no field reversals can be generated.

Finally, we discuss some statistical properties of the decay rate measured by the projection method. The decay rate τ varies from one realization to the other, as displayed in Fig. 3. The standard deviation σ of τ is displayed in Fig. 6. It increases in the vicinity of the onset of the dynamo instability. Values of up to 50 percent are achieved for the fluctuations over the mean, $\sigma\tau^{-1}$. This explains why large samples are required to converge the decay rate close to the dynamo onset.

We acknowledge our colleagues of the VKS team with whom the experimental data used here have been obtained.

-
- [1] Ya. B. Zeldovich, A. A. Ruzmaikin, and D. D. Sokoloff, *Magnetic fields in astrophysics* (Gordon and Breach, New York, 1983).
- [2] F. Pétrélis, N. Mordant, and S. Fauve, *Geophys. Astrophys. Fluid Dyn.* **101**, 289 (2007).
- [3] F. Pétrélis and A. Alexakis, *Phys. Rev. Lett.* **108**, 014501 (2012).
- [4] A. Tilgner, *Phys. Rev. E* **66**, 017304 (2002).
- [5] F. Ravelet, M. Berhanu, R. Monchaux, S. Aumaître, A. Chiffaudel, F. Daviaud, B. Dubrulle, M. Bourgoin, Ph. Odier, N. Plihon, J.-F. Pinton, R. Volk, S. Fauve, N. Mordant, and F. Pétrélis, *Phys. Rev. Lett.* **101**, 074502 (2008).
- [6] C. J. P. Gissinger, *Europhys. Lett.* **87**, 39002 (2009).
- [7] R. Monchaux, M. Berhanu, S. Aumaître, A. Chiffaudel, F. Daviaud, B. Dubrulle, F. Ravelet, S. Fauve, N. Mordant, F. Pétrélis, M. Bourgoin, Ph. Odier, J.-F. Pinton, N. Plihon, and R. Volk, *Phys. Fluids* **21**, 035108 (2009).
- [8] M. Berhanu, R. Monchaux, S. Fauve, N. Mordant, F. Pétrélis, A. Chiffaudel, F. Daviaud, B. Dubrulle, L. Marié, F. Ravelet, M. Bourgoin, Ph. Odier, J.-F. Pinton, and R. Volk, *Europhys. Lett.* **77**, 59001 (2007).
- [9] C. Gissinger, *Phys. Rev. E* **82**, 056302 (2010).
- [10] N. L. Peffley, A. B. Cawthorne, and D. P. Lathrop, *Phys. Rev. E* **61**, 5287 (2000).
- [11] S. Miralles, N. Bonnefoy, M. Bourgoin, Ph. Odier, J.-F. Pinton, N. Plihon, G. Verhille, J. Boisson, F. Daviaud, and B. Dubrulle, *Phys. Rev. E* **88**, 013002 (2013).
- [12] Mechanical constraints prohibit long measurements to be performed at rotation frequencies smaller than 8 Hz.
- [13] F. Pétrélis and S. Fauve, *J. Phys. Condens. Matter* **20**, 494203 (2008); F. Pétrélis, S. Fauve, E. Dormy, and J.-P. Valet, *Phys. Rev. Lett.* **102**, 144503 (2009).